Finite Element Analysis of Electric Field and Particle Transport Phenomena in a Electrostatic Precipitator

H. Nouri, Y. Zebboudj
Laboratoire de Génie Electrique de Bejaia (LGEB)
Université de Bejaia, 06000,
Algeria
E-mail address: hm_nouri@yahoo.fr

N. Zouzou , E. Moreau, L. Dascalescu
Institut Pprime, CNRS, ENSMA
Université de Poitiers
F86962 Futuroscope Chasseneuil Cedex, France
E-mail address:noureddine.zouzou@univ-poitiers.fr

1 Abstract— This paper aims at analysis of the monopolar ionized field in electrostatic precipitator (ESP). An iterative finite-element technique is used to solve Poisons equation. We proposed the introduction of a potential corresponding to the critical minimum ionization field directly in the finite element formulation as a Dirichlet condition. The theoretical migration velocity is obtained by balancing the drag force with the Coulomb force or Electrostatic force acting on a particle. We used the model introduced by Cochet for predicting a particle charge. The model assumes that a particle of the same size attains an equivalent maximum amount of charge for a charging time equal to infinity.

Keywords: Corona discharge, Finite element method, Electric field, Particle velocity

2 Introduction

The ESP operates in the three-step process: charging the particles under nonuniform very high electric field strength, collecting the charged particles on the collecting surface and cleaning the collected particles by washing the collecting electrode with liquid.

Corona discharge, as applied to electrostatic precipitators, is a gas discharge phenomenon associated with the ionization of gas molecules by high-energy electrons in a region of the strong electric field strength. The process of corona generation in the air at atmospheric conditions requires a nonuniform electrical field, which can be obtained by the use of a small diameter wire electrode and a plate or cylinder as the other electrode. An application of a high voltage to the wire results in a production of a high electric field, which reduces significantly with the increasing distant away from the surface of the wire. The reduced electric field near the collecting electrode thus helps to prevent an initiation of the electric arc or sparking due to the electron bridging across the interelectrode spaces. In contrast to the wire-plate system, a uniform electric field is generated between two parallel electrodes, which is more likely to lead to an electrical sparkover due to no limitation of electron avalanche by the reduced electric field [1,2].

This paper presents a numerical algorithm which can be used to simulate the essential parameters of the process in the wires – two planes configuration, including the electric field, the space charge, the current density and the theoretical migration velocity.

3 Mathematical modelling of electrostatic precipitator

The corona phenomenon are obtained from the following relations [3]

$$\nabla \vec{E} = \rho / \varepsilon_0 \tag{1}$$

$$\nabla \vec{J} = 0 \tag{2}$$

$$\vec{J} = \rho . \mu . \vec{E} \tag{3}$$

$$\vec{E} = -\nabla \Phi \tag{4}$$

where $\vec{E}$ is the electric field intensity vector (V/m), ρ is the space charge density (C/m^3), $\vec{J}$ is the current density vector (A/m^2), Φ is the electric potential, ε_0 is the permittivity of free space and μ is the ion mobility ($1.85 \times 10^{-4} m^2 V^{-1} s^{-1}$.

Equations (1)-(4) are, respectively, Poisson's equation, the current continuity condition, the equation of current density and the equation relating the electric field to the potential. These differential equations must be solved for the potential Φ and the

space-charge density ρ, both being functions of the space coordinates.

In reality, it is extremely difficult to find an exact solution to these equations due to their nonlinear nature. However, there are analytical solutions for simple geometries such as spherical and coaxial configurations. All attempts at solving these differential equations have been based on some simplifying assumptions [2, 4].

The most common ones are the following.

(i) The entire electrode spacing is filled with monopolar space-charge of the same polarity as the coronating conductor. The thickness of the ionization layer around the conductor is sufficiently small to be disregarded with respect to the interelectrode spacing.

(ii) The space-charge affects only the magnitude and not the direction of the electric field. This assumption was suggested at first by Deutsch and later referred to as'Deutsch's assumption'.

(iii) The mobility of ions is constant (independent of field intensity).

(iv) Diffusion of ions is neglected.

(v) The surface field of the coronating conductor remains constant at the onset value E_0, which is known as Kaptzov's assumption [5]. For the conductor-to-two plane configurations, E_0 is expressed in kilovolts per centimetre as

$$E_0 = \frac{U}{H \ln(H/r_0)} \tag{5}$$

where r_0 is the conductor radius in centimetres, U is the applied voltage and H is the distance between the wire and the collector plate.

In the present analysis, the electric field at the surface of the coronation conductor,

$$E_{crit} = E_0 f_1(U/V_0) \tag{6}$$

where the function f_1 is assumed to have the following form [2]:

$$f_1 = 1.1339 - 0.16678\left(\frac{U}{V_0}\right) + 0.03\left(\frac{U}{V_0}\right)^2 \tag{7}$$

In conductor-two planes configuration V_0 is given as

$$V_0 = E_0 r_0 \ln(2H/r_0) \tag{8}$$

Solution of equations (1)-(4), which describes the space-charge ionized field, requires three boundary conditions.

(i) The potential on the coronating conductor is equal to the applied voltage.

(ii) The potential on the grounded electrode is zero.

(iii) The magnitude of the electric field at the surface of the coronating conductor E_{crit} is assumed to be a function of the applied voltage.

Many attempts have been made to solve the ionized field problem using the finite-element technique (FET) [1 - 4]. None of them included particle velocity in the solution of the describing equations. A few attempts have included particle charge but using other numerical techniques.

In the present paper, the monopolar ionized field equations are solved in wires-two planes configurations. An iterative FET is used as a numerical tool to solve Poisson's equation and is supported by two algorithms. In the fist algorithm, the current continuity condition is satisfied, neglecting ion diffusion, using a modified characteristics method. In the second, the current continuity condition is satisfied by applying Kirchhoff's current-balance law at each node of the FE grid.

4 Proposed method of analysis

The solution of the space charge field for wire- duct precipitators is described in the following sections. The investigated wire-two planes configuration has a Wire radius r_0 and height H above the ground plane (see Fig. 1).

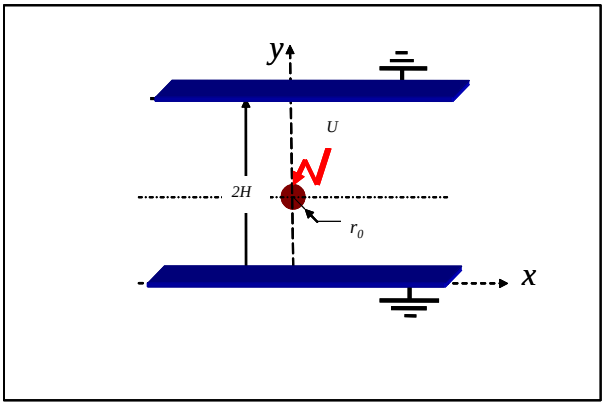

Figure 1. Electrostatic precipitator configurations

The proposed method of analysis is described in the following procedure (Fig.2).

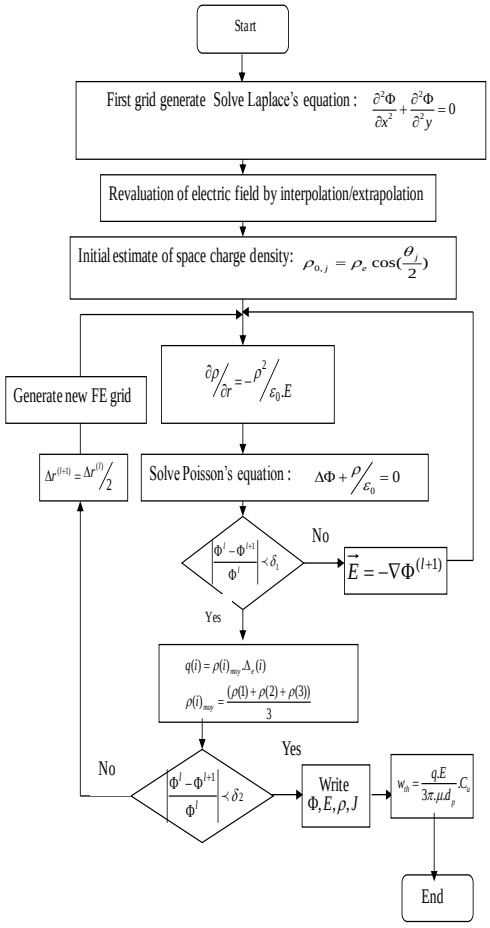

Figure 2. Flow chart of the solution method

The solution process involves the following steps:
Step1: The first mesh is created in the absence of space charge and, therefore, the electric field is Laplacian.

Step 2

Solve via the finite-element method the Laplace equation for Φ ($\Delta\Phi=0$). The potential at the jth boundary is expressed as

$$\Phi_i=\sum_{j=1}^{chg.number}C_{ij}q_j \tag{9}$$

where C_{ij} is the potential coefficient of the charge q_j at the jth point and is equal to

$$C_{ij}=\frac{1}{2\pi\varepsilon_o}\ln\left[\frac{r_j^{'}}{r_j}\right] \tag{10}$$

r_j And $r_j^{'}$ are distances from the ith point to the charge q_j and to its image.

Step 3

The space charge density located at node (*i*,1) around the periphery of the ionization region is assumed initially as:

$$\rho_{i1}=\rho_e\cos(\theta_i/2) \tag{11}$$

where $\rho_e=\rho_0\frac{H}{r_0}\frac{E_0}{E_{crit}}$ (12)

$$\rho_0=[4\varepsilon_0V_s(U-V_s)]\Big/[H^2U(5-4(V_s/U))] \tag{13}$$

$$V_s=E_{cr}.r_0\ln\left[\frac{\sinh(\pi H/a)}{\pi r_0/a}\right] \tag{14}$$

and θ_i is the angle at which the field line emanates at the wire surface [6].

Step 4

The evaluation of the space charge density. From the current continuity equation we can write

$$\nabla J=0\Rightarrow\nabla[\rho(\mu E)]=0\Rightarrow(\nabla\rho)(\mu E)+\rho\mu\nabla E=0 \tag{15}$$

(1) and (15) $\Rightarrow\nabla\rho=\frac{-\rho^2}{\varepsilon_0 E}$ (16)

Along field lines, the Eq.16 becomes [7, 8]

$$\frac{\partial\rho}{\partial r}=\frac{-\rho^2}{\varepsilon_0 E} \tag{17}$$

Integration of eq. 17 gives values of the space charge density along field lines. For the resolution of Eq.17, we used the Runge-Kutta method [9].

Step 5

Using the FEM, solve Poisson's equation, eq. 1. The potential φ within each element is approximated as a linear function of coordinate:

$$\varphi=\varphi_1w_1+\varphi_2w_2+\varphi_3w_3 \tag{18}$$

With *1*, *2*, and *3* representing the nodes of the element ***e*** Fig.3, and *w* is the corresponding shape function [10].

A functional R^e is for mulcted in the usual FEM:

$$R^e=-\int_A[W]^T\left[\left(\frac{\partial\varphi}{\partial x}\right)^2+\left(\frac{\partial\varphi}{\partial y}\right)^2+\rho/\varepsilon_0\right]dA \tag{19}$$

where *A* is the area of triangular element, [*W*] is the row vector containing the elements shapes functions.

Equation (19) is transformed into linear equation by minimizing the functional R^e, in the form:

$$[K].[\Phi] = \{F\} \quad (20)$$

where $$[K] = \sum_{e=1}^{Elt.Num} k_{ij}(e) \quad (21)$$

$$\{F\} = \sum_{e=1}^{Elt.Num} f_i(e) \quad (22)$$

$$k_{ij} = \iint_{\Delta_e} [\frac{\partial N_i}{\partial x}\frac{\partial N_j}{\partial y} + \frac{\partial N_i}{\partial y}\frac{\partial N_j}{\partial x}]dxdy \quad (23)$$

$$f_i = \sum_n \iint_{(e_i)_n} \frac{\rho_i}{\varepsilon_0} N_i dx.dy \quad (24)$$

$$N_i(x, y) = \frac{1}{2.\Delta_e}(a_i + b_i x + c_i y)\,;\ i = 1, 2, 3\,. \quad (25)$$

Note that $N_i(x_j, y_j)$ is the shape function and the coefficients of a_i, b_i and c_i can be easily determined from the definition of the shape function in the finite element theory.

Step 6

Calculate the electric field distribution from the potential using the interpolation/extrapolation method along each field line[11].

4.1 Particle charge phenomena

In intermediate range of particle sizes (0.1-1 μm), both diffusion and field charging mechanisms contribute significantly to charge on the particles leading to a more complex charging equation.

The theoretical analysis of field charging is generally made with three simplifying assumptions that are:

1) The particles are spherical,
2) The field from one particle does not modify that in the proximity of another particle,
3) The particles and ions are suspended in a region permeated by a constant electric field.

The first combined charging model introduced by Cochet (1961) for predicting charge on each particle is shown in Equation 26. The model assumes that a particle of the same size attains an equivalent maximum amount of charge (q) for a charging time equal to infinity[12,13].

$$q = \left[\left(1 + \frac{2\lambda}{d_p}\right)^2 + \left(\frac{2}{1 + 2\lambda/d_p}\right)\left(\frac{\varepsilon_r - 1}{\varepsilon_r + 2}\right)\right]\pi\varepsilon_0.d_p^2.E \quad (26)$$

where λ is the mean free path of gas ions (m) and E is the pseudo-homogeneous electric field strength (V/m).

4.2 Particle transport phenomena

The theoretical migration velocity is obtained by balancing the drag force with the Coulomb force or Electrostatic force acting on a particle. Under a steady-state condition and in the Stokes regime, the theoretical migration velocity is expressed by Equation 27 [13].

$$w_{th} = \frac{q.E}{3\pi.\mu.d_p}.C_u \quad (27)$$

where C_u is the Cunningham correction factor and μ is the gas dynamic viscosity (kg/m.s).

5 Results and discussion

The physical dimensions are wires height H = 5,0 cm, radius $r_0 = 0{,}2$ mm, with a base plane length of 20 cm. The ion mobility was set at $\mu = 1.85 \times 10^{-4} m^2 V^{-1} s^{-1}$. The surface factor η is equal to 1. The grid is generated from the intersection of field lines with equipotential contours see Fig.3. This is called field mapping.

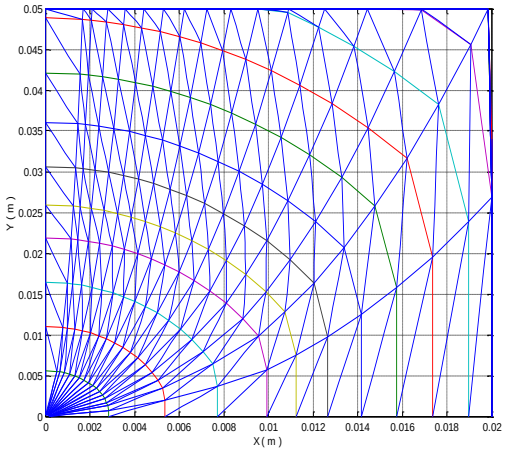

Figure 3 . Generated grid for a precipitator.

The distribution of electric field is shown in figure 4.

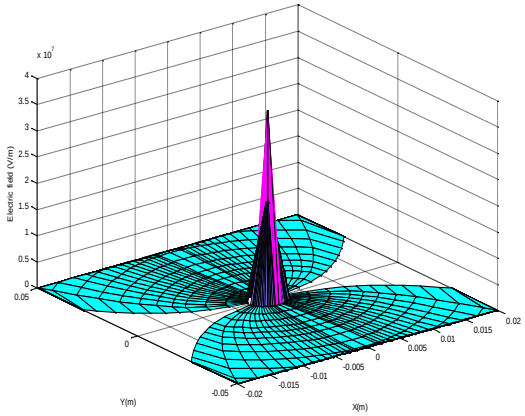

Figure 4. Distribution of electric field

The calculated distributions of electric field at the ground plane are shown in figures 5 and 6.

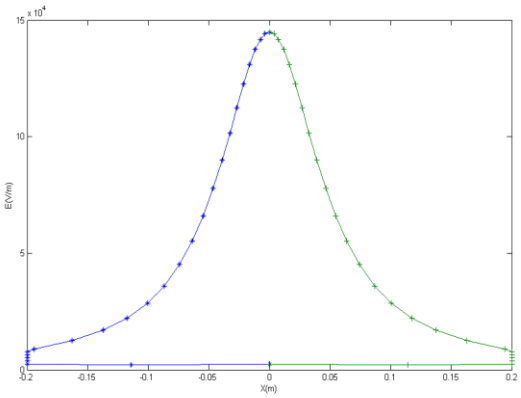

Figure 5. Electric field at the ground plane

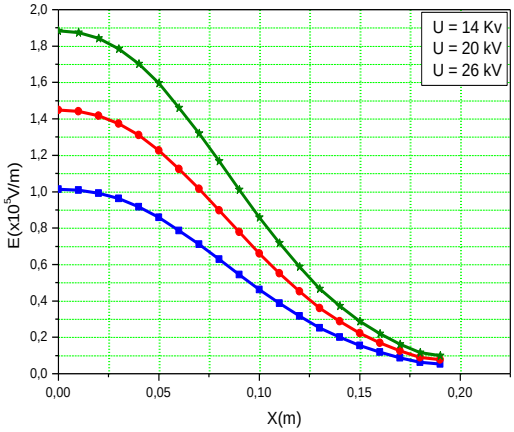

Figure 6. Electric field at the ground plane for different distance and different voltage

In this study, the pseudo-homogeneous electric field strength representing a rough estimate of the real electrical state in the ESP was used for calculating the particle charge (figure 7)and the particle theoretical migration velocity (figure 8) in all the tested models.

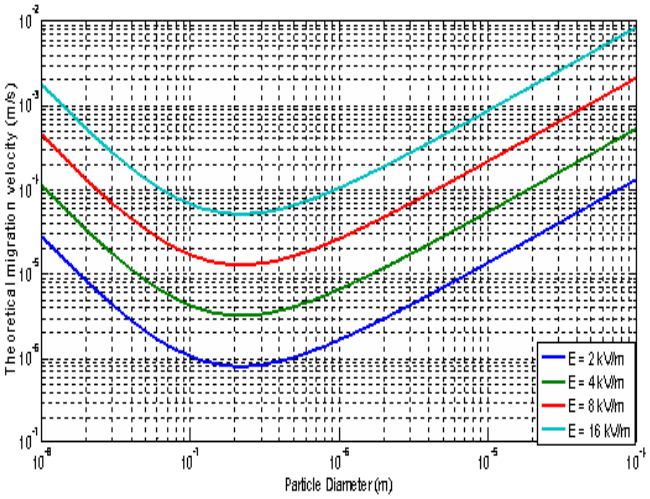

Figure 7. Variation of particles charge with diameter for different values of electric field

(λ = 0,065µm, $\varepsilon_r = 4{,}5$, T = 20°C)

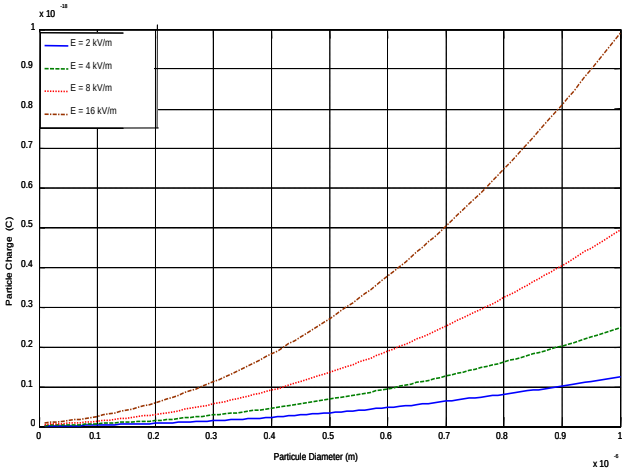

Figure 8 Variation of migration velocity with the size of particles ($\lambda = 0{,}065\,\mu m$,

$\eta = 1{,}85\times10^{-5} kg/m.s$ et T = 20°C).

The Cochet charging equation assumes the charging time to be infinity, which may not be realistic in this experiment where the residence time

is 0.1 s, therefore more likely leading to an over prediction of the collection efficiency for particles smaller than 40 nm. The measured values are substantially higher than the predicted values using the original Deutsch equation with the Robinson charging assumption for particles of all sizes. However, the model results show the same trend of the collection efficiency as a function of particle diameters as that obtained from the measurement. The predicted values using the laminar model with Robinson assumption show better agreement with the measured values for particle diameters less than 40 nm.

6 Conclusion

In the present work, the finite element method is shown to be uniformly applicable to all the equations describing the problem of electric field in corona devices. Using the Newman and Dirichlet boundary conditions method enables quadratical convergence of steady-state solutions such that they are obtained in a few steps.

The proposed numerical computation takes into account the thickness of the ionisation region whereas previous works of this problem ignored this parameter. We integrate the potential correspondent to the minimum ionization field directly in the formulation of the FEM on the border of the ionization region, which reduces the algorithm computation.

The electric field vector is the sum of the field due to the voltage applied at the transmission line plus the field contribution of the continuous space charge distribution. The predicted results indicate that the particles were pushed away from the discharge electrode towards the collecting wall due to the effect of corona winds, which is consistent with the actual particle concentration profile displayed in the photograph reported by previous studies.

REFERENCES

[1] L. Zhao, K. Adamiak, "EHD flow in air produced by electric corona discharging in pin-plate configuration", Journal of Electrostatics, 63, 2005, p.p. 337-350.

[2] Abdel- Salam M. and AL- Hamouz, Analysis of Monopolar Ionized Field as influenced by Ion Diffusion, IEEE Transactions on industry applications, vol. 31, No. 3, 1995.

[3] A.J.Medelin, R.Morrow, C.A.J.Fletche, A pseudotransient approach to steady state solution of electric field-space charge coupled problems, Journal of Electrostatics 43, 1997.

[4] Z. M. Al- Hamouz, A combined algorithm based on finite elements and a modified method of characteristics for the analysis of the corona in wire duct Electrostatic precipitators, IEEE Transactions on industry applications, vol. 38, No. 1, 2002.

[5] N. A. Kaptzov, Elekricheskie invlentia v gazakh i vakuumme, OGIZ, Moscow, p.p. 587 – 630, 1947.

[6] Abdel Salam M., Wiitanen D., Calculation of corona onset voltage for duct– type precipitators, IEEE Trans. On ind. App. Vol. 29, N° 2, 1993.

[7] H. Yala, A. Kasdi, Y. Zebboudj, Analysis of current and electric field distributions beneath a positive DC wire-to-plane corona, The European Physical Journal AP, 21, 2003, p.p. 45-

[8] K. Adamiak, Adaptative approach to finite element modelling of corona fields, IEEE Transactions on industry applications, vol. 30, No. 2, 1994.

[9] L. M. Skvortsov, Diagonally implicit Runge-Kutta metods for stiff problems, Computational mathematics and mathematical physics, Vol. 46, No. 12, p.p. 2110 – 2123, 2006.

[10] H. Nouri, Y. Zebboudj, Analysis of positive corona in wire-to-plate electrostatic precipitator. The European Physical Journal, Applied Physics 49, 11001, 2010.

[11] N. Oussalah, Y. Zebboudj, Negative corona Computation in air, Engineering with computers, Springer, 2006, 21, p.p. 296- 303.

[12] P. Saiyasitpanich, Control of Diesel Particulate and Gaseous Emissions Using a Single-Stage Tubular Wet Electrostatic Precipitator, Thesis of University of Cincinnati, 2006**.**

[13] W. C. Hinds, Aerosol technology: Properties, Behavior and Measurement of airborne particles, 2nd Eddition, John Wiley 1Sons, Inc., New York, 1999.